

## Morphological Control of Chromophore Spin State in Zinc Porphyrin-Peptide Assemblies

Harry Christopher Fry, Lee Andrew Solomon, Benjamin T. Diroll, Yuzi Liu, David J Gosztola, and Hannah M. Cohn

*J. Am. Chem. Soc.*, **Just Accepted Manuscript** • DOI: 10.1021/jacs.9b09935 • Publication Date (Web): 09 Dec 2019

Downloaded from [pubs.acs.org](https://pubs.acs.org) on December 17, 2019

### Just Accepted

“Just Accepted” manuscripts have been peer-reviewed and accepted for publication. They are posted online prior to technical editing, formatting for publication and author proofing. The American Chemical Society provides “Just Accepted” as a service to the research community to expedite the dissemination of scientific material as soon as possible after acceptance. “Just Accepted” manuscripts appear in full in PDF format accompanied by an HTML abstract. “Just Accepted” manuscripts have been fully peer reviewed, but should not be considered the official version of record. They are citable by the Digital Object Identifier (DOI®). “Just Accepted” is an optional service offered to authors. Therefore, the “Just Accepted” Web site may not include all articles that will be published in the journal. After a manuscript is technically edited and formatted, it will be removed from the “Just Accepted” Web site and published as an ASAP article. Note that technical editing may introduce minor changes to the manuscript text and/or graphics which could affect content, and all legal disclaimers and ethical guidelines that apply to the journal pertain. ACS cannot be held responsible for errors or consequences arising from the use of information contained in these “Just Accepted” manuscripts.

# Morphological Control of Chromophore Spin State in Zinc Porphyrin-Peptide Assemblies

H. Christopher Fry\*, Lee A. Solomon, Benjamin T. Diroll, Yuzi Liu, David J. Gosztola, Hannah M. Cohn.

Center for Nanoscale Materials, Argonne National Laboratory, 9700 South Cass Ave., Argonne, IL 60439.

Supporting Information Placeholder

**ABSTRACT:** Self-assembled peptide micelles and fibers demonstrate unique control over the photophysical properties of the bound, light-activated chromophore, zinc protoporphyrin IX, (PPIX)Zn. Micelles encapsulate either a mixture of uncoordinated and coordinated (PPIX)Zn or all coordinated depending on the ratio of peptide:porphyrin. As the ratio increases toward a 1:1 micelle:porphyrin ratio, providing the chromophore with a discrete coordination environment reminiscent of unstructured proteins, the micelles favor triplet formation. Fibers, on the other hand promote a linear array of porphyrin molecules that dictates exciton hopping and excimer formation at ratios as high as 60:1, peptide:porphyrin. However, even in fibers, the formation of the triplet species increases with increasing peptide:porphyrin ratio due to increased spatial separation between neighboring chromophores facilitating intersystem crossing. Full characterization of the micelles structures and comparison to the fibers lead to the comparison with natural systems and the ability to control the excited populations that have utility in photocatalytic processes. In addition, the incorporation of a second chromophore, heme, yields an electron transfer pathway in both micelles and fibers that highlights the utility of the peptide assemblies when engineering multichromophore arrays as inspired by natural, photosynthetic proteins.

## Introduction

Controlling the photophysical state of arranged chromophores is crucial for developing abiotic light harvesting assemblies and photocatalysts that are dependent on the photoexcited state spin conformation. Natural light harvesting assemblies are comprised of a precise arrangement of cofactors that efficiently capture sunlight and convert it into energy.<sup>1-3</sup> The protein scaffold responsible for this organization of chromophores evolved over eons arriving at the structure employed by proteins today, notably photosystem I, II (PSI, PSII) and light harvesting complex I, II (LHCI, LHCI).<sup>4-5</sup> The chlorophyll molecules alone possess different photophysical behavior than the organized molecules within the complex protein assemblies highlighting the importance of the protein scaffold in the engineering of efficient light harvesting systems.<sup>6-9</sup> Furthermore, individual chlorophyll molecules have been identified in proteins like cytochrome *b6f* serving as a photoprotectant from reactive oxygen species with distinct photodynamic behavior from larger light harvesting assemblies.<sup>10</sup> Each protein organizes either an array of molecules or isolates individual molecules in order to obtain a specific photoinitiated process.

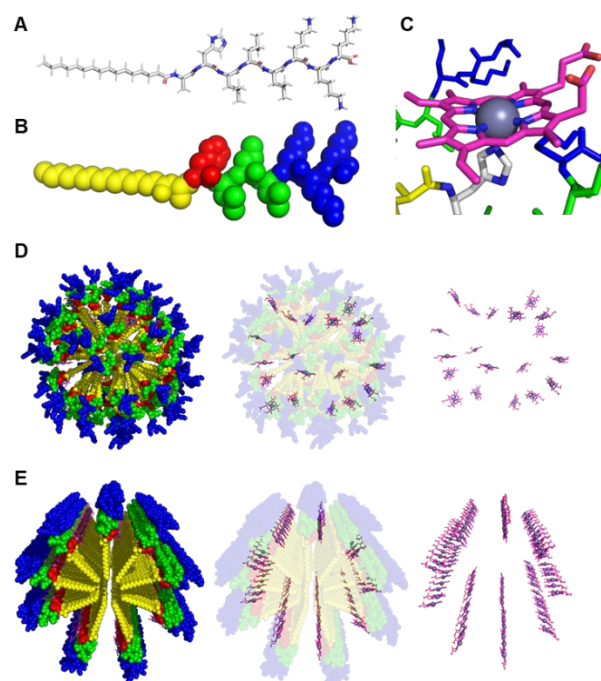


**Figure 1.** Molecular components: c16AHL<sub>3</sub>K<sub>3</sub>-CO<sub>2</sub>H monomer in A. stick and B. sphere (hydrogens removed for clarity) representations, C. (PPIX)Zn axially coordinated to histidine in stick representation (hydrogens removed for clarity). Cartoon representation of the D. micelle assembly at a 5:1 peptide:(PPIX)Zn ratio and E. fiber assembly at a 6:1 peptide: (PPIX)Zn ratio. Amino acid color code: Blue, lysine; green, leucine; red, histidine; yellow, palmitoyl capped

Nature's precise molecular placement of chromophores in antenna complexes has inspired the development of many soft matter light harvesting materials<sup>11</sup> and led investigations towards the dependence of the materials' photophysical behavior on morphology and chromophore arrangement.<sup>12-18</sup> Peptide fibers have been found to arrange the light harvesting molecule zinc protoporphyrin IX in a linear array such that exciton hopping occurs along the axis of the fiber on a picosecond timescale.<sup>19-21</sup> This differs from the photophysical behavior of (PPIX)Zn in organic solvents or (PPIX)Zn myoglobin where a long lived triplet state (milliseconds) is observed.<sup>22</sup> In the examples of the fibers, exciton migration is essential for shuttling charge over long distances. However, controlling the triplet yield of zinc porphyrin molecules is important in the formation of long lived charge separated states.<sup>23</sup> Therefore, when developing new light

harvesting materials or photocatalysts, demonstrating control over the excited state(s) is crucial.

Previously, we demonstrated the importance of morphology on heme catalysis.<sup>24</sup> Peroxidase activity was demonstrated in micelles containing heme but diminished in fibers. Here, we demonstrate the importance of morphology on controlling the photophysical processes of (PPIX)Zn. Essentially, fibers yield a linear arrangement of (PPIX)Zn molecules facilitating exciton hopping; whereas, micelles yield bound but mostly isolated (PPIX)Zn molecules allowing for triplet formation. In addition, we demonstrate that triplet formation is obtainable in fibers, but the amount of (PPIX)Zn must be significantly decreased to effectively separate neighboring pairs of molecules.

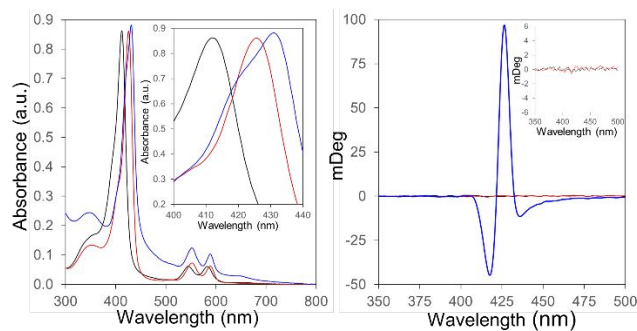


**Figure 2.** A. UV/visible and B. circular dichroism spectroscopy of (PPIX)Zn (100 mM NH<sub>4</sub>OH, pH 11, black line), (PPIX)Zn:Peptide Micelle (HEPES, pH 7, red line), (PPIX)Zn:Peptide Fibers (100 mM NH<sub>4</sub>OH, pH 11, blue line). Inset A: expanded Soret region. Inset B: smaller y-axis range for free (PPIX)Zn and (PPIX)Zn:Micelle.

## Results and Discussion

**Morphology Control:** The morphology of the peptide amphiphile c16-AHL<sub>3</sub>K<sub>3</sub>-CO<sub>2</sub>H (Figure 1A,B) can be controlled between micelles and fibers<sup>24</sup> where the (PPIX)Zn molecules (Figure 1C) is coordinated by a histidine residue. All samples are prepared stepwise by first assembling the peptide followed by addition of (PPIX)Zn (See Materials and Methods section for more detail). In 50 mM HEPES buffer at pH 7, micelles form that are comprised of peptides in a random coil conformation as indicated by the negative  $\pi$ - $\pi^*$  transition at 200 nm in the circular dichroism spectrum, Figure S1.<sup>25</sup> At pH 11 (100 mM NH<sub>4</sub>OH) twisted, parallel  $\beta$ -sheet rich fibers form as indicated by the red shifted and intense positive  $n$ - $\pi^*$  transition at 203 nm and negative  $\pi$ - $\pi^*$  transition at 223 nm, Figure S1.<sup>26</sup>

UV/visible spectroscopy highlights the ability to coordinate the light harvesting molecule (PPIX)Zn to both morphologies (figure 2A) while circular dichroism comments on chiral orientation of neighboring chromophores<sup>27</sup> (figure 2B). Interestingly, when comparing the UV/visible spectra of the micelle bound chromophore to the fiber bound chromophore, we note a distinct difference. In micelles, the narrow symmetric peak centered at 425 nm (figure 2A) combined with the lack of chiral signature (figure 2B) suggests that the chromophores, while bound, are in a disordered state relative to one another. In fibers, the split Soret (421 & 431 nm, figure 2A inset) of the UV/vis spectrum in conjunction with the intense exciton coupling found by CD spectroscopy (figure 2B) suggests that the (PPIX)Zn molecules are bound in a highly ordered array, i.e. fixed dihedral angles between neighboring chromophores. While previous reports have detailed

the photophysical processes of (PPIX)Zn in the fiber construct,<sup>19-21</sup> we have neither reported on the (PPIX)Zn micelle construct nor the ability to control the relative populations of singlet, excimer and triplet. The ability to control these populations is essential for designing photocatalytic and photoconductive materials. We demonstrate here that by controlling the concentration of (PPIX)Zn in the material, we can control the population of the triplet state in both micelles and fibers.

Dynamic light scattering of filtered samples at various concentrations in HEPES buffer in the absence of (PPIX)Zn (the apo-state) yields ~ 6 nm micelles. Upon introducing (PPIX)Zn at a peptide:porphyrin ratio of 6:1 the micelle size increases to ~30 nm. Interestingly, when the ratio increases from 6:1 to 60:1, the micelle size decreases from ~30 nm to ~6 nm, Figure S3. Atomic force microscopy and transmission electron microscopy confirms the micelle and fiber formation and highlights a similar range in observed sizes, Figure S2. The observed change in micellar size as a function of peptide:(PPIX)Zn ratio is due to the balancing of competing forces. In the absence of the porphyrin, the micelle forms due to: (1) the hydrophobic collapse of the structure due to the palmitoyl (c16) tail yielding a hydrophobic core and (2) electrostatic repulsion between the neighboring, positively charged lysine head groups consistent with atomistic and coarse grained simulations.<sup>28</sup> Upon incorporating (PPIX)Zn, additional forces are introduced: (1) the macrocycle possesses two negatively charged carboxyl moieties which introduces a favorable electrostatic interaction that contributes to the aggregation of neighboring micelles and (2) (PPIX)Zn-histidine coordination. Since the electrostatic repulsion between neighboring lysine groups is responsible for the micelle assembly, we hypothesize that the larger sizes at a 6:1 ratio are due to electrostatic interactions between the negatively charged chromophore and the positively charged peptide. In fact, the zeta potential measurements of the peptide in HEPES buffer yielded  $\zeta = 19.5 \pm 2.8$  while (PPIX)Zn yielded  $\zeta = -25.1 \pm 1.8$ . The charge balancing of the peptide and the chromophore facilitates the formation of small aggregates. As the ratio increases to 60:1 the positive charge on the lysine head groups overwhelms the negative carboxyl side groups of the macrocycle yielding a narrower distribution of micelles similar to the apo micelles, figure S3. The fiber formation is simpler. The hydrophobic collapse due to the palmitoyl (c16) tail occurs first followed by the neutralization of the lysine amine groups ( $pK_a = 10.7$ ) by adjusting the pH to 11 with ammonium hydroxide. This reduces electrostatic repulsion between neighboring peptides and facilitates the formation of  $\beta$ -sheet rich fibers as observed by CD spectroscopy (Figure S1) and AFM (Figure S2).

Our crude model (Figure 1D) highlights 76 peptide molecules forming a single micelle while reports suggest that this and similar peptides form micelles comprised of 40 - 50 molecules.<sup>28-29</sup> At 6:1 and 10:1, 8 to 12 porphyrins are taken up by each micelle. At a 20:1 ratio, only 2 to 4 porphyrins are bound to each micelle whereas 60:1 would potentially yield micelles with a single porphyrin molecule coordinated (a Poisson distribution with  $\lambda = 1$ ). This range allows us to investigate the photodynamics of micelles that contain (PPIX)Zn in a range of loading capacities within a single micelle.

**Steady State Spectroscopy:** To investigate the loading of the light activated chromophore (PPIX)Zn into peptide micelles, we explore samples prepared at various ratios of peptide to (PPIX)Zn: 0:1, 6:1, 10:1, 20:1, 30:1, and 60:1. Effectively, the amount of porphyrin molecule per micelle decreases with increasing ratio such that the micelle at 6:1 is grossly packed and at 60:1 there is approximately one porphyrin per micelle. The electronic

absorption spectrum of (PPIX)Zn in HEPES buffer (50 mM HEPES, 100 mM NaCl, pH 7.0) without peptide yields a Soret band at 403 nm and Q-bands at 557, 590 nm, Figure 3A & S4. Upon addition of the peptide, the high energy transition shifts 23 nm to 426 nm and the low energy bands to 551, 589 nm typical of histidine axial ligation.<sup>30</sup> Micelles readily pass through filters. In the absence of the peptide, (PPIX)Zn aggregates and is efficiently removed via sample filtration, Figure S4. Filtered samples of micelles at a 6:1 peptide:porphyrin ratio (0.2  $\mu$ m PTFE filter, Fisherbrand) indicate the presence of both the uncoordinated and coordinated species at 403 and 426 nm respectively suggesting that the micelles encapsulate the (PPIX)Zn molecule even when the molecule is not coordinated to histidine, Figure S4. This mixture of uncoordinated and coordinated states at low ratios is simply due to an “overcrowding” of chromophores in a single micelle. Upon increasing the ratio to 60:1, a transition to micelles where all of the (PPIX)Zn molecules are histidine coordinated is observed as indicated by the narrow Soret band at 425 nm, Figure 3A. At high ratios, the porphyrin molecule is isolated with few neighboring chromophores within a single micelle. By carefully titrating the peptide into a solution of (PPIX)Zn, we determined the binding constant to be 14.3  $\mu$ M with a stoichiometry of  $\sim$  5:1 peptide:porphyrin, Figure S5.

(PPIX)Zn coordination to fibers (formed at pH 11) has been described in earlier reports.<sup>19-21</sup> (PPIX)Zn under basic conditions is more soluble than in micelle forming conditions (HEPES buffer) and yields a Soret band at 412 nm, Figure 3B. At a 6:1 ratio, the Soret band is split into peaks at 421 and 431 nm. Since both peaks are red shifted from the solubilized (PPIX)Zn peak at 412 nm, we attribute this split Soret to a slip-stacked arrangement of neighboring chromophores.<sup>31</sup> Notably, the dissociation constant ( $K_D$ ) is nearly two orders of magnitude less (0.23  $\mu$ M) than the micelle binding constant.<sup>21</sup> As the ratio increases, the number of porphyrin units per fiber decreases resulting in fewer neighboring chromophores. This is reflected in the absorption spectra where the peaks at 421 and 431 nm shift to 425 nm and the FWHM narrows, Figure 3B. At a ratio of 60:1, the Soret band has transitioned to a single peak at 425 nm with greater intensity consistent with many reports of slip-stacked porphyrin assemblies compared to the individual porphyrin unit.<sup>31</sup> In fact, the spectrum of the fibers at 60:1 peptide:porphyrin ratio more closely resembles the spectrum of the micelles at 60:1. Under these conditions, the porphyrin units are spatially segregated and resemble that of a histidine coordinated (PPIX)Zn molecule in myoglobin.<sup>22</sup>

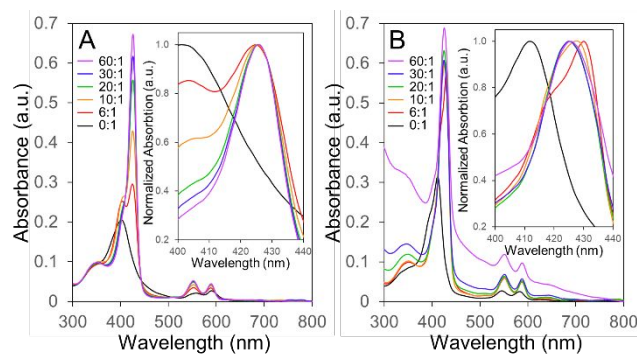


**Figure 3.** UV/visible spectroscopy of (PPIX)Zn coordinated to A. micelles and B. fibers at increasing ratios of peptide:porphyrin. [(PPIX)Zn] = 25  $\mu$ M. Black, 0:1; red, 6:1; orange, 10:1; green, 20:1; blue, 30:1; purple, 60:1. Inset: Normalized spectra in the Soret region to highlight spectral

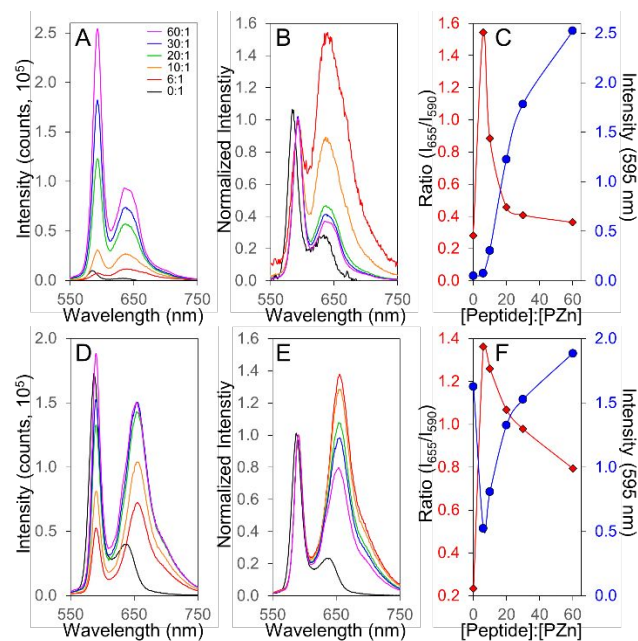


**Figure 4.** Fluorescence spectroscopy of micelles (A - C) and fibers (D - F) with (PPIX)Zn at various ratios: 0:1, black; 6:1, red; 10:1, orange; 20:1, green; 30:1, blue; 60:1, purple. A & D represent the emission spectra, B & E represent the normalized (at 590 nm) emission spectra, C & F represent plots of the peptide: (PPIX)Zn versus peak intensity ( $I_{655}/I_{590}$ ) (red diamonds, left axis) and 595 alone nm (blue circles, right axis).

Fluorescence spectroscopy of the assembly comments on the chromophore arrangement. We previously demonstrated that an excimer forms that emits at 680 nm and when mixed with the singlet spectrum yields an apparent increase of the peak at 655 nm yielding a spectrum in which the peak at 655 nm is more intense than the peak at 590 nm.<sup>20</sup> This phenomenon occurs as a result of the 1D nanofibers enforcing a cofacial arrangement between neighboring chromophores facilitating the orientation required for excimer formation. This is in opposition to the 0D nature of the micelle that binds, but does not organize the metalloporphyrins with a controlled orientation or specific periodicity. Therefore, we expect to see fewer excimers forming in micelles than in fibers. As we decrease the number of porphyrin molecules per assembly (micelles or fibers), we expect fewer interactions between neighboring chromophores and concomitantly a lower excimer population that is reflected in a decrease in the plotted ratio of peak intensities,  $I_{655\text{ nm}}/I_{590\text{ nm}}$ . In our experiments, the samples were excited at a wavelength that exhibited little change in the absorption spectrum upon addition of peptide,  $\lambda_{\text{ex}} = 409$  nm (micelles) or  $\lambda_{\text{ex}} = 414$  nm (fibers). In the absence of the peptide in HEPES buffer, (PPIX)Zn aggregates and therefore yields an emission spectrum typical of a quenched, aggregated species, Figure 4A&B. As peptide is added, the intensity of the emission increases and indicates that the peptide is breaking up the porphyrin aggregates. At low ratios of peptide:porphyrin (6:1 and 10:1), where (PPIX)Zn is found in both the coordinated and uncoordinated states in the micelle, the lower energy peak at 645 nm is more intense than the higher energy 590 nm peak. This is similar to what is observed in the fiber but could correlate to energy transfer between the coordinated and uncoordinated species and quite possibly the formation of an excimer. At higher ratios, (> 20:1) a typical (PPIX)Zn singlet spectrum is obtained as indicated by an increase in the emission intensity and the lower peak ratio

value ( $I_{655 \text{ nm}}/I_{590 \text{ nm}}$ ), Figure 4C. At pH 11, (PPIX)Zn is more soluble and yields an intense emission spectrum that upon addition of peptide (6:1 ratio) decreases due to close packing of neighboring chromophores. Upon increasing the peptide concentration, the emission intensity increases suggesting a decrease in chromophore-chromophore interactions, Figure 4D&E. Interestingly, the decrease in the peak ratio is less dramatic in fibers when compared to micelles, Figure 4F. This indicates a more gradual decrease in excimer population where a pure singlet species is never observed. The steady state fluorescence spectra indicate the importance of morphology on the distribution of excited state population. Micelles at low loading of porphyrin achieve a typical singlet spectrum whereas fibers have a significant contribution from the excimer state due to the linear, 1D arrangement of chromophores.

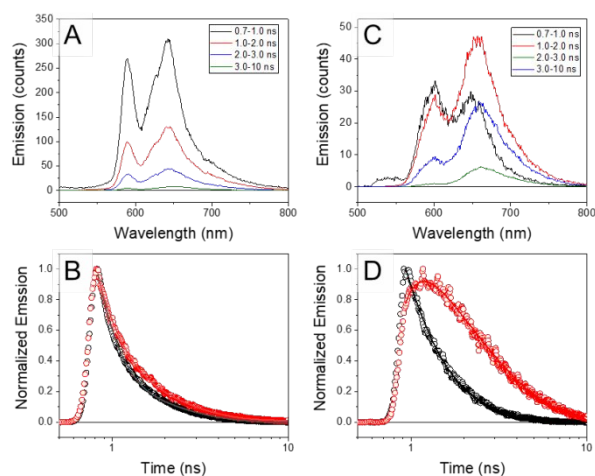


**Figure 5.** TRPL spectroscopy ( $\lambda_{\text{ex}} = 425 \text{ nm}$ ) of 10:1 (peptide):(PPIX)Zn micelles (A,B) and fibers (C,D). Transient emission spectra of micelles (A) and fibers (C) averaged over delay times: 0.7 – 1.0 ns, black; 1.0 – 2.0 ns, red; 2.0 – 3.0 ns, blue; and 3.0 – 10.0 ns, green. Kinetics of micelles (B) and fibers (D) monitored at 590 nm (black) and 690 nm (red).

**Time resolved spectroscopy:** It is essential to understand the temporal relationships between the excited states if they are to be employed as materials. Fortunately, zinc porphyrins are extremely well characterized as both molecules and assemblies.<sup>32-34</sup> Typically, upon excitation into the Soret band of (PPIX)Zn, a singlet state forms and undergoes internal conversion on the femtosecond timescale ( $S_2 \rightarrow S_1$ ,  $\tau_{\text{IC}} < 100 \text{ fs}$ ). The singlet can then undergo non-radiative relaxation to the ground state or intersystem crossing ( $S_1 \rightarrow T_1$ ,  $\tau_{\text{ISC}} \sim 2 \text{ ns}$ ) forming the long lived triplet state ( $T_1 \rightarrow S_0$ ,  $\tau = 5 - 10 \text{ ms}$ ).<sup>22</sup> Supramolecular arrangement of zinc porphyrin molecules yield highly modulated lifetimes due to energy transfer and interchromophore hopping events that arise from molecules in close proximity to one another. Here, we employ the peptide morphology to control the population of these various excited states.

To investigate this distribution of states, the amount of (PPIX)Zn added to the assembled peptide was varied 6:1, 10:1, 20:1, 30:1, and 60:1. Essentially, the range of assemblies coordinates anywhere from 19 to 1 (PPIX)Zn molecule per micelle. Upon excitation into the Soret band ( $\lambda_{\text{ex}} = 425 \text{ nm}$ ), both micelles and fibers demonstrate behavior suggesting a mixture of (PPIX)Zn in aggregated/arranged states (ps lifetimes) and monomeric states (> ns lifetimes). Time resolved photoluminescence monitors the radiative states of the assemblies and can comment on the singlet

to ground state ( $S_1 \rightarrow S_0$ ) fluorescence. Aggregated states impact the lifetime when compared to the monomeric singlet state. Transient absorption detects all species: singlet, triplet, excimer, and stimulated emission from some of those states. Here, we are interested in how efficiently we form the long lived triplet state and what the morphological factors that control it are. Therefore, it is essential to investigate the primary factors that are limiting or promoting triplet formation.

**Time resolved Photoluminescence (TRPL):** The photodynamics of (PPIX)Zn in micelles versus fibers are considerably different. When the peptide:porphyrin ratio is 10:1 in micelles, a majority of the porphyrin is coordinated to histidine while the remaining molecules are uncoordinated. The samples are excited at 425 nm to ensure that a majority of the molecules being “activated” are histidine coordinated (PPIX)Zn molecules. Interestingly, the kinetics are biexponential ( $\tau_1 = 300 \text{ ps}$ , 85%;  $\tau_2 = 1.5 \text{ ns}$ , 15%) but wavelength independent (Figure 5A,B) and suggests that the photophysics is dominated by fast energy transfer while a small contribution represents a singlet undergoing intersystem crossing. This is in opposition to the fibers at a 10:1 ratio where all porphyrin molecules are coordinated, but the kinetics are largely wavelength dependent such that the kinetics at 590 nm are similar to that found for the micelle, but at 690 nm we see the growth of the excimer (Figure 5C,D). While the excimer in the fiber is analyzed in greater detail in previous work,<sup>20</sup> it is important to show that the micelle yields entirely different behavior (Figure 5A vs. 5C), i.e. the lack of

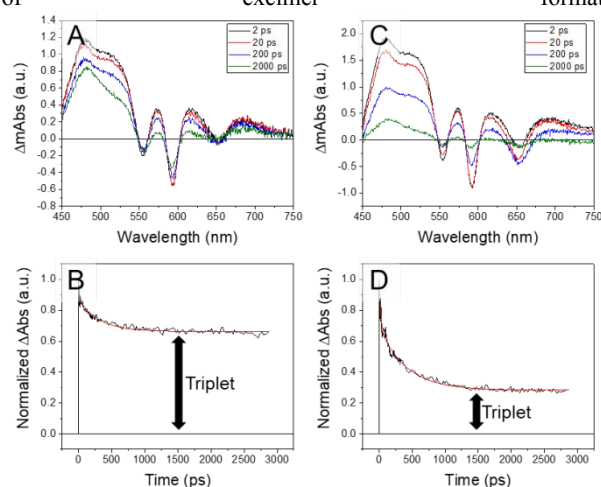


**Figure 6.** TA spectroscopy ( $\lambda_{\text{ex}} = 425 \text{ nm}$ ) of peptide:(PPIX)Zn (6:1) micelles (A – difference spectra, B – kinetics at 500 nm) and fibers (C – difference spectra, D – kinetics at 500 nm). Difference spectra (A & C) are presented at delay times of 2 (black), 20 (red), 200 (blue), and 2000 (green) ps.

When the photophysical properties of (PPIX)Zn in fibers were investigated, it was noted that high doping levels (6:1 peptide:porphyrin) led to increased excimer formation but shorter hopping intervals and low doping levels (60:1) led to decreased excimer formation and longer hopping intervals following a 1D exciton hopping model.<sup>20</sup> In micelles, the excimer does not form as it does in the fibers. In fact, micelles demonstrate a preference toward the (PPIX)Zn molecules behaving like isolated porphyrin molecules where intersystem crossing to the triplet is indicated by an increase in the contribution from the longer lived kinetic component ( $\tau_{\text{ISC}} = \tau_2 = 1.5 \text{ ns}$ ) as the amount of peptide is increased from 6:1 to 60:1, Figure S6 & S7. At 6:1, micelles possess a mixture of coordinated and uncoordinated (PPIX)Zn. As a result, the longer

lifetime contribution  $\tau_2$  is the lowest ( $\sim 5\%$ ) suggesting that energy transfer between neighboring molecules is likely. At 20:1, all (PPIX)Zn molecules ( $\sim 2 - 4$  per micelle) are coordinated to histidine, but potential for neighboring porphyrins to undergo energy transfer exists such that the  $\tau_2$  contribution is  $\sim 50\%$ . At 60:1, each micelle binds approximately one (PPIX)Zn molecules. The  $\tau_2$  contribution is  $\sim 97\%$  and is attributed to near quantitative intersystem crossing forming the triplet state. This high conversion to the triplet was not observed in fibers.

**Transient Absorption Spectroscopy (TA):** TRPL is advantageous in some regards as it limits detection to emissive species. TA, on the other hand, yields more complicated spectra because the singlet, triplet, and excimer species are all detected with overlapping features in the difference spectra. Nonetheless, the difference between micelles and fibers becomes more clear because the (PPIX)Zn triplet species is long lived ( $\tau = 5 - 10$  ms) and easily detect by TA.

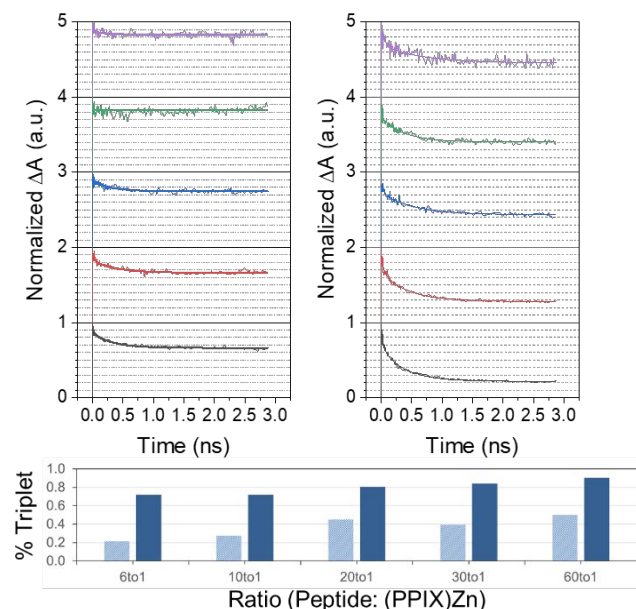


**Figure 7.** Transient absorption kinetics ( $\lambda_{\text{ex}} = 425$  nm,  $\lambda_{\text{mon}} = 500$  nm) of (A) micelles and (B) fibers monitored at varying ratios of Peptide: (PPIX)Zn. 6:1, black; 10:1, red; 20:1, blue; 30:1, green; 60:1, purple. (C) Triplet population, determined from percentage of residual absorption at 2.5 ns, of (PPIX)Zn in fibers (light blue) and micelles (dark blue) at various peptide:(PPIX)Zn ratios.

The micelles demonstrate a single exponential, picosecond decay lifetime that we attribute to hopping between neighboring molecules ( $\tau_{\text{Hop}} = 173 \pm 30$  ps) similar in magnitude to that found in TRPL, Figure 6 A&B. As we increase the amount of peptide to afford samples in which one micelle contains one (PPIX)Zn molecule (60:1), we find that this picosecond process is nearly eliminated due to the fact that energy hopping between close neighbors is less likely to occur consistent with TRPL, Figure 7. The lifetime extends beyond the 2.5 ns time window of the experiment. The long lived excited state is assigned as the triplet. The amount of triplet formed is determined by the percentage of residual absorption. An increase in triplet formation directly correlates to fewer (PPIX)Zn molecules per assembly.

When (PPIX)Zn is coordinated to the nanofibers, we find a dramatic change in the photophysical properties, Figure 6C&D.

We have previously demonstrated that fiber formation and (PPIX)Zn doping level of these samples yield controllable exciton hopping that is dictated by the quantity of excimer formation.<sup>20</sup> The multiexponential kinetics suggest competing processes. Here, we wish to highlight that upon increasing the peptide concentration, where we effectively increase the intermolecular spacing between neighboring chromophores, an observed increase in triplet formation occurs. Triplet formation is indicated via the residual absorption at 2.5 ns, Figure 6C&D. Therefore, when (PPIX)Zn is most densely packed in the nanofiber (peptide:porphyrin at 6:1), we observe less than 20% triplet formation. This means that more than 80% of the porphyrin molecules are involved in exciton hopping/excimer formation events. As we decrease the amount of porphyrin loaded in the peptide fibers (60:1), increasing the distance between the nearest porphyrin neighbors, we observe a controlled increase in the triplet formation to nearly 50%, Figure 7. The amount of triplet formed is less than the corresponding micelle samples, but the general trend of increasing triplet population with fewer porphyrins loaded in the assemblies is consistent.

Dependence of the photophysical properties of zinc porphyrins has been investigated in other soft material platforms. For example, dendrimers are capable of assembling into 0D and 1D nanoscale objects. Zinc porphyrin units are attached covalently in dendrimer assemblies and yield a host of tailorable photophysical properties, but typically require synthetic modification to achieve the desired properties.<sup>13</sup> Another example is that of surfactant assisted self-assembly of zinc tetrapyrrolyl porphyrin (ZnTPyP).<sup>35</sup> Conditions were found that yielded 0D nanospheres with negligible photocatalytic activity, whereas 1D nanofibers (similar composition, different assembly conditions) demonstrate photocatalytic decomposition of rhodamine B.<sup>14</sup> Through electron paramagnetic resonance spectroscopy, the nanospheres were found to produce singlet oxygen in an energy transfer process and the nanofibers produced superoxide or hydroxyl radical via electron transfer which highlights the importance of controlling the photophysical properties to produce the desired function.

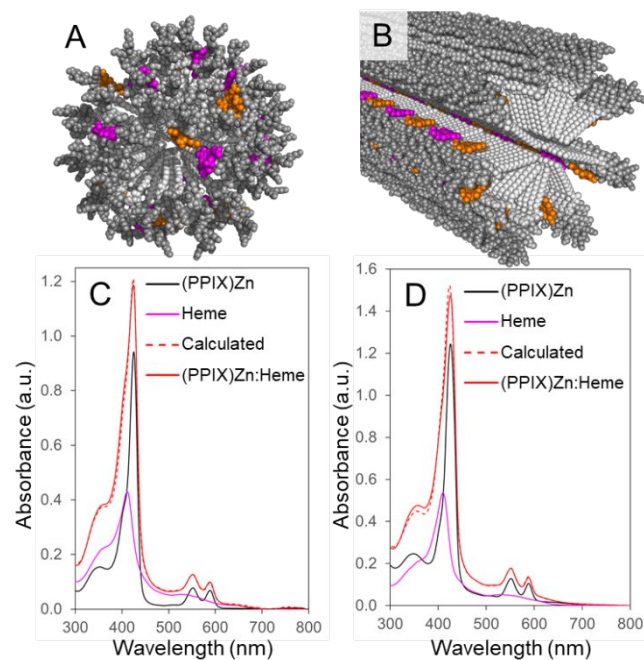


**Figure 8.** Cartoon depiction of grayscale micelle (A) and fiber (B) with coordinated (PPIX)Zn (purple) and heme (orange) molecules. Representative UV/visible spectra of chromophores

coordinated to micelles (C) and fibers (D). 20:1 c16AHL<sub>3</sub>K<sub>3</sub>-CO<sub>2</sub>H:(PPIX)Zn (black), 20:1 c16AHL<sub>3</sub>K<sub>3</sub>-CO<sub>2</sub>H:Heme (magenta), 20:1:1 c16AHL<sub>3</sub>K<sub>3</sub>-CO<sub>2</sub>H:(PPIX)Zn:Heme (red), calculated addition spectrum of (PPIX)Zn only + Heme only (dashed red spectrum).

#### Adding a second cofactor, heme, leads to electron transfer:

While we demonstrate the behavior of a single chromophore in our materials, natural light harvesting systems organize many chromophores, e.g. chlorophyll, carotenoids, plastoquinone, and heme. The other cofactors act as electron acceptors and photoprotectants necessary to carry out the entire photosynthetic mechanism. The peptide presented here has been demonstrated to bind and modulate the photophysical properties of (PPIX)Zn and has been shown previously to bind and tune the catalytic activity of heme. In an effort to explore energy transfer between two chromophores within a single self-assembled peptide structure, heme has been added to “underloaded” peptide:(PPIX)Zn micelles and fibers, Figure 8A&B.

First, (PPIX)Zn and Heme ((PPIX)Fe<sup>III</sup>) are demonstrated to bind within a single peptide construct, fibers or micelles. The preferred ratio of peptide:cofactor is 5:1 in micelles and 6:1 in fibers. Therefore, fibers or micelles comprised of 20:1 c16AHL<sub>3</sub>K<sub>3</sub>-CO<sub>2</sub>H:(PPIX)Zn are “underloaded”. As a result, heme can be backfilled into the available binding sites leading to a statistical distributions of both (PPIX)Zn and heme in a single assembly. Upon addition of heme (25 μM) to a sample containing c16AHL<sub>3</sub>K<sub>3</sub>-CO<sub>2</sub>H:(PPIX)Zn (500 μM:25 μM) we find an increase in the peak intensity at 425 nm in both assemblies, Figure 8C&D. Similarly, c16AHL<sub>3</sub>K<sub>3</sub>-CO<sub>2</sub>H:Heme (500 μM:25 μM) is characterized with a Soret peak at λ<sub>max</sub> = 412 nm in micelles and 409 nm in fibers consistent with previous reports. Upon addition of (PPIX)Zn (25 μM), an increase in the intensity at 425 nm indicates successful coordination to the assembly. By comparing the spectrum representing the sample containing both (PPIX)Zn and heme with the calculated spectrum where we add the two spectra of the samples containing only (PPIX)Zn and only heme, good agreement is found emphasizing successful binding of the two molecules in micelles and fibers, Figure 8.

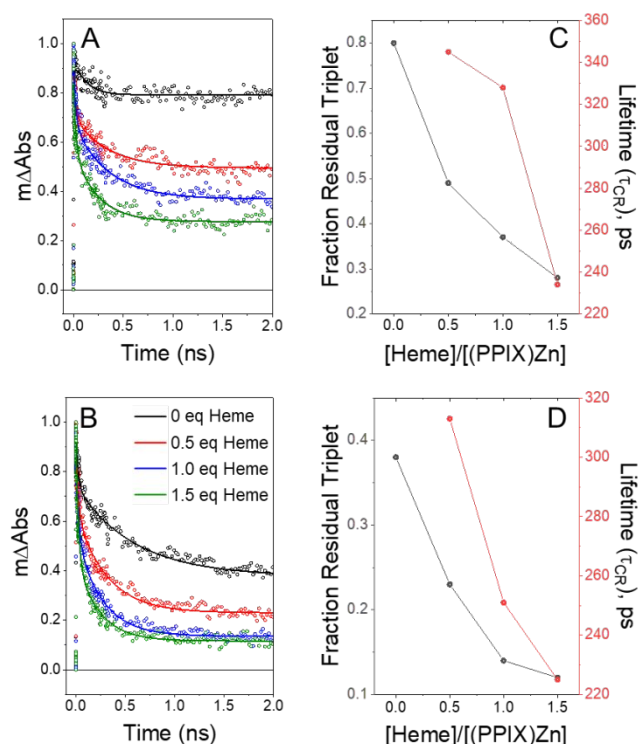


**Figure 9.** Transient absorption ( $\lambda_{\text{ex}} = 425$  nm) kinetics measured at  $\lambda = 500$  nm in micelles (A) and fibers (B) at varying ratios of [Heme]/[(PPIX)Zn]: 0, black; 0.5, red; 1.0, blue; 1.5, green. Charge recombination lifetimes ( $\tau_{\text{CR}}$ ) and fraction of residual triplet found with respect to [Heme]/[(PPIX)Zn] ratios in micelles (C) and fibers (D).

Functionally, ferric heme, (PPIX)Fe<sup>III</sup>, can act as an electron acceptor to photoexcited (PPIX)Zn yielding (PPIX)Fe<sup>II</sup> and (PPIX)<sup>+</sup>Zn.<sup>36</sup> Steady state fluorescence spectroscopy highlights the quenching of the (PPIX)Zn singlet state in micelles and the (PPIX)Zn singlet and excimer mixture in fibers upon addition of heme, which implicates charge transfer as a likely mechanism. By introducing 0.5, 1.0 and 1.5 eq of heme (with respect to (PPIX)Zn), the emission spectrum becomes increasingly quenched in both micelles and fibers, Figure S8. Transient absorption studies ( $\lambda_{\text{ex}} = 425$  nm) of the same samples show similar difference spectra that do not explicitly indicate the presence of ferrous heme, (PPIX)Fe<sup>II</sup>, Figure S9. While the features in the difference spectra are similar to those where only (PPIX)Zn is present, Figure S10, there is a noticeable increase in absorption at 680 nm which may indicate the presence of the cation radical, (PPIX)Zn<sup>+</sup>. Further support of electron transfer is found where the charge recombination lifetime ( $\tau_{\text{CR}}$ ) decreases upon increasing heme concentration, Figure 9. As the heme concentration is increased fewer metalloporphyrin binding sites remain forcing the two chromophores to be physically close to one another and as a result yields increasingly shorter lifetimes in both micelles and fibers. Furthermore, the observed residual triplet absorption at time = 2 ns decreases with respect to increasing heme concentration. This is consistent with the emission quenching studies and suggests that the presence of heme facilitates electron transfer.

Our results differ from long range electron transfer studies in proteins where the rates of tunneling through the protein are strongly distant dependent.<sup>37</sup> In fact, a recent study by Kajihara et al. investigated the electron transfer within a supramolecular assembly of modified (PPIX)Zn and Heme substituted cytochrome

$b_{562}$ .<sup>36</sup> The assemblies make long chains where the porphyrin units are separated by 3 nm. Charge separation occurs between triplet (PPIX)Zn and ferric heme (PFe<sup>III</sup>) to yield PZn<sup>+</sup> and PFe<sup>II</sup>. In this assembly, typical charge recombination rates on the order of 100s of milliseconds to 1 second were found consistent with long range electron transfer in biological systems. The presented time dependent studies differ from these published works simply because the self-assembled, peptide micelles and fibers do not yield a specific, defined distance between donor and acceptor. In a 6:1 ratio sample, assuming all of the chromophores were evenly distributed, the edge to edge distance is  $\sim 1.8$  nm, Figure S10. This would translate to  $\tau_{CR} \sim 1$   $\mu$ s. Alternatively, the interchromophore distance could be near van der Waals contact yielding picosecond lifetimes. Molecular assemblies of synthetic zinc porphyrin and iron porphyrin dyads where the distances are  $< 1$  nm report picosecond timescale rates of recombination.<sup>38-41</sup> Our reported values ( $\tau_{CR}$ -micelles  $\sim 235$  ps and  $\tau_{CR}$ -fibres  $\sim 225$  ps at 20:1:1.5 peptide:PZn:PFe or  $\sim 7:1$  peptide:chromophore, figure 9 C,D) imply that the heme and (PPIX)Zn are closer together on average than the “even distribution” distance of 1.8 nm. Future work will include a more in depth analysis at longer time scales to identify potential long range electron processes that were not detected on the ultrafast time scale regime.

Here, micelles and fibers were demonstrated to control the relative population of the triplet state, but the energy transfer process is initiated by the formation of the (PPIX)Zn singlet state which occurs in both constructs. While the peptide:(PPIX)Zn:Heme materials behave similarly regardless of morphology, the ability to incorporate two molecules highlights the adaptability of the self-assembled peptides to create artificial photosynthetic constructs where the quantity of cofactor can be doped in as needed to tune the efficiency of the final material.

## Conclusion

The peptide assemblies presented here are unique compared to both synthetic and naturally occurring light harvesting arrays. Due to the non-covalent nature of our assembly, we can control the density of the chromophores in the array and modulate the probability of the excited state undergoing intersystem crossing to the triplet. In addition, a second chromophore, heme, can be added to facilitate efficient energy transfer. Systematic control of chromophore incorporation is not possible in many synthetic light harvesting arrays as their constructs are limited/dictated by the molecular synthon. Isolated natural systems highlight specific numbers of chlorophyll molecules, and reconstitution of chlorophyll in natural systems is difficult due to the structural complexity of the large proteins. The simple peptide amphiphile sequence has the spatial precision needed for effective light harvesting complexes but offers ease of cofactor incorporation allowing for facile benchtop preparation. Furthermore, the micellar and fibrillar nature of these assemblies make them amenable for material applications such as interfacing with controlled layer deposition for the production of novel solar conversion materials.

All in all, we have demonstrated the ability to control the amount of triplet formed as a function of material morphology and chromophore density. Micelles yield a greater triplet population due to the lower presence of paired (PPIX)Zn neighbors. Fibers, consistent with our previous description, organize chromophores in long-range ordered arrays resulting in the formation of excimers preventing intersystem crossing and therefore decreasing the triplet population. However, in both micelles and fibers, we can increase the triplet population simply by decreasing the number of porphyrin units loaded in the assembly. This work holds potential insight into

controlling photocatalytic reactions at the interface with either the micelle or fiber constructs. Introduction of the heme molecule to the peptide:(PPIX)Zn assemblies highlights the successful engineering of energy transfer in both micelles and fibers. Future work will further explore the introduction of additional cofactors within the micelle and fiber constructs in an effort to produce more complex systems reminiscent of natural systems that incorporate multiple cofactors for cascading catalytic processes.

## Materials and Methods

*Chemicals and Reagents:* Amino acids and resins were purchased from Chem Impex International. All other chemicals and reagents used in this work were purchased from Sigma-Aldrich unless otherwise noted.

*Peptide Synthesis, Purification, and Characterization:* The synthetic procedure for c16-AHL<sub>3</sub>K<sub>3</sub>-CO<sub>2</sub>H has been reported in our previous studies.[Ref 19,20,24]

*Sample/Stock Solution Preparation:* The purified peptide, c16-AHL<sub>3</sub>K<sub>3</sub>-CO<sub>2</sub>H (3-4 mg) was dissolved in nanopure water (Millipore A10) to obtain a 1 wt% solution, c16-AHL<sub>3</sub>K<sub>3</sub>-CO<sub>2</sub>H (1 wt%, 8.4 mM). (PPIX)Zn was dissolved in DMSO to achieve a 10 mM stock solution in an opaque eppendorf tube to prevent photodegradation. Note: (PPIX)Zn/DMSO stock solutions were always made to ensure that the final DMSO concentration in the sample was less than 1% (v/v). Samples for experiments were prepared by dissolving the peptide in 50 mM HEPES, 100 mM NaCl, pH 7.0 buffer for micelles or in 100mM NH<sub>4</sub>OH for fibers and heating at 90°C for five minutes. Samples were removed from heat, (PPIX)Zn was added, and the samples reheated at 90°C for an additional five minutes. The introduction of heme was identical to that for (PPIX)Zn. The sample concentrations are reported in Table S1.

*Micelle and Fiber Size Determination:* Dynamic light scattering measurements were performed on a Zetasizer Nano (Malvern Instruments) in a 1 cm disposable plastic cuvette. Atomic force microscopy (Veeco Multimode 8) was performed using the Scanasyt peak force tapping mode in a liquid holder equipped with a silicon tip on a nitride lever (Cantilever - Scanasyt-Fluid+, Bruker). A 100  $\mu$ L drop of the sample (1500 mM c16AHL<sub>3</sub>K<sub>3</sub>-CO<sub>2</sub>H (apo) and 1500 mM c16AHL<sub>3</sub>K<sub>3</sub>-CO<sub>2</sub>H:25 mM (PPIX)Zn (holo) samples diluted 10 fold) was deposited on freshly cleaved mica and incubated at room temperature for 15 minutes. The sample solution was removed via micropipette and replaced with a fresh droplet (30  $\mu$ L) of the assembly solvent, e.g. HEPES buffer for micelles and 10 mM NH<sub>4</sub>OH for fibers. Areas of 2  $\mu$ m<sup>2</sup> were collected at a rate of 1 Hz per line (512 lines). Transmission electron microscopy of the holo samples was performed on a JEM 2100F (Jeol Ltd.). The samples were identical to those used in the liquid AFM measurement. 10  $\mu$ L of the sample was drop cast on a lacey carbon copper grid (Ted Pella Inc.). After 5 minutes the droplet was wicked with filter paper. The sample containing the micelles was stained with 1 wt% phosphotungstic acid for 5 minutes. The excess stain was wicked with filter paper followed by three washes with water (3 x 10 mL) and wicked with filter paper. The TEM grids were then dried under ambient conditions.

*Steady State Spectroscopy:* Electronic absorption spectra were collected on a Cary 50 (Varian, Inc.) at 1 nm intervals from 300 to 800 nm. Circular dichroism spectroscopy were collected on a J-815 spectropolarimeter (Jasco, Inc.) at 0.1 nm intervals from 190-260 nm for analyzing peptide secondary structure and from 350 – 500 nm for analyzing chromophore/porphyrin supramolecular arrangement. Emission spectra were collected on a Nanolog

spectrofluorometer (Horiba Scientific) from 500 to 750 nm. Samples for fluorescence were diluted tenfold (300  $\mu\text{L}$  to 3000  $\mu\text{L}$  in respective solvents for micelles or fibers) from the values in Table S1 and were placed in a 1 cm quartz cuvette.

**Time Resolved Spectroscopy:** Streak Camera Photoluminescence. Time- and wavelength-resolved photoluminescence (trPL) data were acquired using a pulsed laser and streak camera detection system. Specifically, a 35-fs pulsewidth, amplified Ti:sapphire laser operating at 2 kHz pumped an optical parametric amplifier to produce 425 nm pump pulses which were directed into the sample. Photoluminescence was collected with a lens and directed to a 150 mm focal length spectrograph and single-photon sensitive streak camera (Hamamatsu). The samples were nitrogen purged in a 2 mm quartz cuvette equipped with a 14/20 ground glass joint and sealed with a rubber septum. The pump power was controlled by a variable neutral density filter and maintained within the linear excitation regime, well below the onset of exciton-exciton annihilation. For each power, measurements were performed with both a short (2 ns) and long (10 ns) time window to capture both the fast dynamics of excimer formation and slow fluorescence decay of ZnP.

Time-resolved transient absorption (TA) measurements were performed with a commercial transient spectrometer (Newport Helios). Pump and probe pulses were derived from a regeneratively amplified Ti:sapphire laser (Newport Tsunami and SpitFire Pro), which produced 120-fs pulses at 5 kHz. A pump wavelength of 425 nm was used for all measurements, while a white light continuum probe was generated from a sapphire crystal. The incident pump power was adjusted with a variable neutral density filter and calibrated with a power meter, and its diameter was determined to be  $\sim 300 \mu\text{m}$  at the sample. Pump fluences were varied within the nonlinear excitation regime, confirmed both by the saturation of the transient absorption signal and the presence of exciton-exciton annihilation. The nitrogen-purged samples were stirred in a 2 mm quartz cuvette during the course of the measurement. Each data set represents an average of 3 measurements. Prior to further analysis, data was chirp-corrected with SurfacePro software, version 4.1.0. Ultrafast Systems, LLC.

The kinetics were fit to either single exponential (eq. 1) or biexponential decay (eq. 2) profiles using Origin Pro 2018 Software. In the case of biexponential fitting, the percent contribution from the two lifetimes was determined by averaging the resulting amplitudes from eq. S2 (eq. 3).

$$y = A1 \cdot \exp(-x/t1) + y0 \quad (\text{eq. 1})$$

A1 is the absorption (or emission) at  $t = 0$ ,  $t1$  is the lifetime,  $y0$  is the residual absorption value,  $x$  is time, and  $y$  is  $\square$ Abs (or emission).

$$y = A1 \cdot \exp(-x/t1) + A2 \cdot \exp(-x/t2) + y0 \quad (\text{eq. S2})$$

A1 is the extrapolated absorption (or emission) at  $t = 0$  for  $t1$ ,  $t1$  is the first (shorter) lifetime, A2 is the extrapolated absorption (or emission) at  $t = 0$  for  $t2$ ,  $t2$  is the second (longer) lifetime,  $y0$  is the residual absorption value,  $x$  is time, and  $y$  is  $\Delta$ Abs (or emission).

Contribution from  $\tau_1$  or  $\tau_2$ ,

$$\tau_1 (\%) = A1/(A1+A2), \tau_2 (\%) = A2/(A1+A2) \quad (\text{eq. S3})$$

## ASSOCIATED CONTENT

### Supporting Information

The Supporting Information is available free of charge on the ACS Publications website. brief description (file type, i.e., PDF)

## AUTHOR INFORMATION

### Corresponding Author

E-mail: hfry@anl.gov

### Present Addresses

Department of Chemistry and Biochemistry, George Mason University, 4400 University Drive, Fairfax, VA 22030 (L. A. S.)

Wellesley College, 106 Central Street, Wellesley, Massachusetts 02481, United States (H.M.C.)

## ACKNOWLEDGMENT

This work was performed at the Center for Nanoscale Materials, a U.S. Department of Energy Office of Science User Facility, and supported by the U.S. Department of Energy, Office of Science, under Contract No. DE-AC02-06CH11357.

## REFERENCES

- Buchel, C., Evolution and function of light harvesting proteins. *J. Plant Physiol.* **2015**, *172*, 62-75.
- Dall'Osto, L.; Bressan, M.; Bassi, R., Biogenesis of light harvesting proteins. *Biochim. Biophys. Acta-Bioenerg.* **2015**, *1847* (9), 861-871.
- Scholes, G. D.; Fleming, G. R.; Olaya-Castro, A.; van Grondelle, R., Lessons from nature about solar light harvesting. *Nat. Chem.* **2011**, *3* (10), 763-774.
- Liu, Z. F.; Yan, H. C.; Wang, K. B.; Kuang, T. Y.; Zhang, J. P.; Gui, L. L.; An, X. M.; Chang, W. R., Crystal structure of spinach major light-harvesting complex at 2.72 angstrom resolution. *Nature* **2004**, *428* (6980), 287-292.
- Nelson, N.; Yocum, C. F., Structure and function of photosystems I and II. *Annu. Rev. Plant Biol.* **2006**, *57*, 521-565.
- Bjorn, L.; Papageorgiou, G. C.; Blankenship, R. E.; Govindjee, A viewpoint: Why chlorophyll a? *Photosynth. Res.* **2009**, *99* (2), 85-98.
- Engel, G. S.; Calhoun, T. R.; Read, E. L.; Ahn, T. K.; Mancal, T.; Cheng, Y. C.; Blankenship, R. E.; Fleming, G. R., Evidence for wavelike energy transfer through quantum coherence in photosynthetic systems. *Nature* **2007**, *446* (7137), 782-786.
- Duan, H. G.; Prokhorenko, V. I.; Cogdell, R. J.; Ashraf, K.; Stevens, A. L.; Thorwart, M.; Miller, R. J. D., Nature does not rely on long-lived electronic quantum coherence for photosynthetic energy transfer. *Proc. Natl. Acad. Sci. U. S. A.* **2017**, *114* (32), 8493-8498.
- Roscioli, J. D.; Ghosh, S.; LaFountain, A. M.; Frank, H. A.; Beck, W. F., Quantum Coherent Excitation Energy Transfer by Carotenoids in Photosynthetic Light Harvesting. *J. Phys. Chem. Lett.* **2017**, *8* (20), 5141-5147.
- Dashdorj, N.; Zhang, H. M.; Kim, H. Y.; Yan, J. S.; Cramer, W. A.; Savikhin, S., The single chlorophyll a molecule in the cytochrome b(6) f complex: Unusual optical properties protect the complex against singlet oxygen. *Biophys. J.* **2005**, *88* (6), 4178-4187.
- Otsuki, J., Supramolecular approach towards light-harvesting materials based on porphyrins and chlorophylls. *J. Mater. Chem. A* **2018**, *6* (16), 6710-6753.
- Jiang, D. L.; Aida, T., Morphology-dependent photochemical events in aryl ether dendrimer porphyrins: Cooperation of

- dendron subunits for singlet energy transduction. *J. Am. Chem. Soc.* **1998**, *120* (42), 10895-10901.
13. Jiang, D. L.; Aida, T., Bioinspired molecular design of functional dendrimers. *Prog. Polym. Sci.* **2005**, *30* (3-4), 403-422.
14. Guo, P. P.; Chen, P. L.; Ma, W. H.; Liu, M. H., Morphology-dependent supramolecular photocatalytic performance of porphyrin nanoassemblies: from molecule to artificial supramolecular nanoantenna. *J. Mater. Chem.* **2012**, *22* (38), 20243-20249.
15. Babu, S. S.; Kartha, K. K.; Ajayaghosh, A., Excited State Processes in Linear pi-System-Based Organogels. *J. Phys. Chem. Lett.* **2010**, *1* (23), 3413-3424.
16. Hwang, I. W.; Park, M.; Ahn, T. K.; Yoon, Z. S.; Ko, D. M.; Kim, D.; Ito, F.; Ishibashi, Y.; Khan, S. R.; Nagasawa, Y.; Miyasaka, H.; Keda, C.; Takahashi, R.; Ogawa, K.; Satake, A.; Kobuke, Y., Excitation-energy migration in self-assembled cyclic zinc(II)-porphyrin arrays: A close mimicry of a natural light-harvesting system. *Chem.-Eur. J.* **2005**, *11* (12), 3753-3761.
17. Das, A.; Molla, M. R.; Maity, B.; Koley, D.; Ghosh, S., Hydrogen-Bonding Induced Alternate Stacking of Donor (D) and Acceptor (A) Chromophores and their Supramolecular Switching to Segregated States. *Chem.-Eur. J.* **2012**, *18* (32), 9849-9859.
18. Kumar, J.; Nakashima, T.; Tsumatori, H.; Kawai, T., Circularly Polarized Luminescence in Chiral Aggregates: Dependence of Morphology on Luminescence Dissymmetry. *J. Phys. Chem. Lett.* **2014**, *5* (2), 316-321.
19. Fry, H. C.; Garcia, J. M.; Medina, M. J.; Ricoy, U. M.; Gosztola, D. J.; Nikiiforov, M. P.; Palmer, L. C.; Stupp, S. I., Self-Assembly of Highly Ordered Peptide Amphiphile Metalloporphyrin Arrays. *J. Am. Chem. Soc.* **2012**, *134* (36), 14646-14649.
20. Solomon, L. A.; Sykes, M. E.; Wu, Y. M. A.; Schaller, R. D.; Wiederrecht, G. P.; Fry, H. C., Tailorable Exciton Transport in Doped Peptide-Amphiphile Assemblies. *ACS Nano* **2017**, *11* (9), 9112-9118.
21. Solomon, L. A.; Wood, A. R.; Sykes, M. E.; Diroll, B. T.; Wiederrecht, G. P.; Schaller, R. D.; Fry, H. C., Microenvironment control of porphyrin binding, organization, and function in peptide nanofiber assemblies. *Nanoscale* **2019**, *11* (12), 5412-5421.
22. Luo, L. Y.; Chang, C. H.; Chen, Y. C.; Wu, T. K.; Diao, E. W. G., Ultrafast relaxation of zinc protoporphyrin encapsulated within apomyoglobin in buffer solutions. *J. Phys. Chem. B* **2007**, *111* (26), 7656-7664.
23. Fukuzumi, S.; Ohkubo, K.; Suenobu, T., Long-Lived Charge Separation and Applications in Artificial Photosynthesis. *Accounts Chem. Res.* **2014**, *47* (5), 1455-1464.
24. Solomon, L. A.; Kronenberg, J. B.; Fry, H. C., Control of Heme Coordination and Catalytic Activity by Conformational Changes in Peptide-Amphiphile Assemblies. *J. Am. Chem. Soc.* **2017**, *139* (25), 8497-8507.
25. Ranjbar, B.; Gill, P., Circular Dichroism Techniques: Biomolecular and Nanostructural Analyses- A Review. *Chem. Biol. Drug Des.* **2009**, *74* (2), 101-120.
26. Manning, M. C.; Illangasekare, M.; Woody, R. W., Circular-dichroism studies of distorted alpha-helices, twisted beta-sheets, and beta turns. *Biophys. Chem.* **1988**, *31* (1-2), 77-86.
27. Pescitelli, G.; Gabriel, S.; Wang, Y. K.; Fleischhauer, J.; Woody, R. W.; Berova, N., Theoretical analysis of the porphyrin-porphyrin exciton interaction in circular dichroism spectra of dimeric tetraarylporphyrins. *J. Am. Chem. Soc.* **2003**, *125* (25), 7613-7628.
28. Deshmukh, S. A.; Solomon, L. A.; Kamath, G.; Fry, H. C.; Sankaranarayanan, S., Water ordering controls the dynamic equilibrium of micelle-fibre formation in self-assembly of peptide amphiphiles. *Nat. Commun.* **2016**, *7*.
29. Israelachvili, J. N.; Mitchell, D. J.; Ninham, B. W., Theory of self-assembly of hydrocarbon amphiphiles into micelles and bilayers. *Journal of the Chemical Society-Faraday Transactions II* **1976**, *72*, 1525-1568.
30. Nappa, M.; Valentine, J. S., Influence of axial ligands on metalloporphyrin visible absorption spectra - complexes of tetraphenylporphyrinato zinc. *J. Am. Chem. Soc.* **1978**, *100* (16), 5075-5080.
31. Satake, A.; Kobuke, Y., Artificial photosynthetic systems: assemblies of slipped cofacial porphyrins and phthalocyanines showing strong electronic coupling. *Org. Biomol. Chem.* **2007**, *5* (11), 1679-1691.
32. Choi, M. S.; Yamazaki, T.; Yamazaki, I.; Aida, T., Bioinspired molecular design of light-harvesting multiporphyrin arrays. *Angew. Chem.-Int. Edit.* **2004**, *43* (2), 150-158.
33. Aratani, N.; Kim, D.; Osuka, A., Discrete Cyclic Porphyrin Arrays as Artificial Light-Harvesting Antenna. *Accounts Chem. Res.* **2009**, *42* (12), 1922-1934.
34. Panda, M. K.; Ladomenou, K.; Coutsolelos, A. G., Porphyrins in bio-inspired transformations: Light-harvesting to solar cell. *Coord. Chem. Rev.* **2012**, *256* (21-22), 2601-2627.
35. Qiu, Y. F.; Chen, P. L.; Liu, M. H., Evolution of Various Porphyrin Nanostructures via an Oil/Aqueous Medium: Controlled Self-Assembly, Further Organization, and Supramolecular Chirality. *J. Am. Chem. Soc.* **2010**, *132* (28), 9644-9652.
36. Kajihara, R.; Oohora, K.; Hayashi, T., Photoinduced electron transfer within supramolecular hemoprotein co-assemblies and heterodimers containing Fe and Zn porphyrins. *J. Inorg. Biochem.* **2019**, *193*, 42-51.
37. Gray, H. B.; Winkler, J. R., Long-range electron transfer. *Proc. Natl. Acad. Sci. U. S. A.* **2005**, *102* (10), 3534-3539.
38. Osuka, A.; Maruyama, K.; Mataga, N.; Asahi, T.; Yamazaki, I.; Tamai, N., Geometry dependence of intramolecular photoinduced electron transfer in synthetic zinc ferric hybrid diporphyrins. *J. Am. Chem. Soc.* **1990**, *112* (12), 4958-4959.
39. Helms, A.; Heiler, D.; McLendon, G., Electron transfer in bis-porphyrin donor-acceptor compounds with polyphenylene spacers shows a weak distance dependence. *J. Am. Chem. Soc.* **1992**, *114* (15), 6227-6238.
40. Duncan, T. V.; Wu, S. P.; Therien, M. J., Ethyne-bridged (porphinato)zinc(II)-(porphinato)iron(III) complexes: Phenomenological dependence of excited-state dynamics upon (porphinato) iron electronic structure. *J. Am. Chem. Soc.* **2006**, *128* (32), 10423-10435.
41. Wasielewski, M. R., Energy, charge, and spin transport in molecules and self-assembled nanostructures inspired by photosynthesis. *J. Org. Chem.* **2006**, *71* (14), 5051-5066.

## TOC Graphic

